Encapsulation of Myoglobin in a Cetyl Trimethylammonium Bromide Micelle in Vacuo: A Simulation Study[†]

Yaofeng Wang,[‡] Daniel S. D. Larsson,[‡] and David van der Spoel*

Department of Cell and Molecular Biology, Uppsala University, Husargatan 3, Box 596, SE-751 24 Uppsala, Sweden

Received October 18, 2008; Revised Manuscript Received December 4, 2008

ABSTRACT: A recently published paper describes encapsulation of myoglobin into cetyl trimethylammonium bromide (CTAB) micelles by electrospray ionization followed by detection using mass spectrometry [Sharon, M., et al. (2007) *J. Am. Chem. Soc. 129*, 8740−8746]. Here we present molecular dynamics simulations aimed at elucidating the structural transitions that accompany the encapsulation and dehydration processes. Myoglobin associates with CTAB surfactants in solution, but no complete reverse micelle is formed. Upon removal of most of the water and exposure of the system to vacuum, a stable protein−surfactant reverse micelle forms. The surfactants shield the protein to a large extent from dehydration-related conformational changes, in the same manner that a water shell does, as previously described by Patriksson et al. [(2007) *Biochemistry 46*, 933−945]. Solvated CTAB micelles undergo a rapid inversion when transported to the gas phase and form very stable reverse micelles, independent of the amount of water present.

Incorporation of proteins into lipid or surfactant micelles allows new inroads for protein characterization and other studies of proteins and macromolecular complexes in the gas phase (*1*). For measurements that have to be performed in vacuum, like mass spectrometry, or new methods that are curently under development, like single-particle imaging using an X-ray free electron laser (FEL)[1] (*2, 3*), encapsulation of proteins into micelles will allow a greater range of subjects to be studied besides soluble particles. Common to these techniques is the fact that sample delivery is nontrivial and the most gentle techniques involve aerosol injection, e.g., electrospray ionization (ESI) (*4, 5*). The sample has to be taken from bulk solution into vacuum through a successive process of dehydration. The understanding of what happens to biomolecules on a structural level during such processes has, foremost, come from in silico studies (*6*−*11*).

Preservation of the native protein conformation in vacuum is fundamentally important for structural studies if they are to be of any relevance to biological systems (*7, 10*). Simulations suggest that protein structure is remarkably well preserved even under the nonphysiological conditions present in ESI (*9*). Via optimization of the design of the experiments, meaningful structural analyses of the sample can be performed, e.g., monitoring the amount of solvent molecules that are noncovalently bound to a protein in the gas phase (*12*). Indeed, a key aspect in general could be to let some residual water remain as a protective film around the sample. A veil of water, just a few water molecules thick, seems to be enough to preserve the hydrogen bonding structure of the outermost parts of the protein (*9*). It has even been suggested that a protective layer of water could prevent or, rather, postpone radiation damage in single-particle bioimaging experiments with X-ray FELs (*2, 3, 13, 14*). One of the major reasons for pursuing novel single-molecule imaging techniques, which have been predicted to yield structural information at resolutions close to atomic resolution based on X-ray scattering (*2*), is the notorious difficulty of studying membrane proteins via X-ray crystallographical techniques. In this context, a micelle covering could provide a membranelike interface for the protein against the surrounding void. Indeed lipid/surfactant micelles are routinely used for solubilizing membrane proteins in X-ray crystallography (*15, 16*).

Surfactants can also form reverse micelles under appropriate conditions, e.g., in organic solvents. The hydrophilic core of such a micelle would offer an excellent shelter for a water soluble protein during ESI. Sharon et al. used mass spectrometry to study horse heart myoglobin (Mb) in complex with cetyl trimethylammonium bromide (CTAB) surfactants under ESI conditions (*17*). By noticing that the counterions of the charged head group of the surfactant molecule were not substituted with other ion species present in the buffer, they drew the conclusion that one holo Mb molecule was embedded in a reverse CTAB micelle which formed during or after the ionization process, and which was stable while solvent was still present in the droplet.

Here we provide an analysis using molecular dynamics simulations of myoglobin in vacuum with and without CTAB surfactants and with varying amounts of water. A reverse

[†] Funding provided by the Swedish Research Council.

* To whom correspondence should be addressed. Telephone: +46-18-4714205. Fax: +46-17-511755. E-mail: spoel@xray.bmc.uu.se.

[‡] These authors contributed equally to this work.

[1] Abbreviations: *A*, area; CTA, cetyl trimethylammonium; CTAB, cetyl trimethylammonium bromide; DSSP, dictionary of secondary structure patterns; ESI, electrospray ionization; FEL, free electron laser; FFT, fast Fourier transform; GROMACS, Groningen Machine for Chemical Simulation; HB, hydrogen bond; LINCS, Linear Constraint Solver; Mb, myoglobin; MD, molecular dynamics; PDB, Protein Data Bank; PME, particle mesh Ewald; R_g, radius of gyration; rmsd, root-mean square deviation; rmsf, root-mean-square fluctuation; SPC, simple point charge.

10.1021/bi801952f CCC: $40.75
Published on Web 01/20/2009

Table 1: Overview of the Simulations[a]

	CTAB micelle				myoglobin			Mb/CTAB		
	0 nm S_{dry}	0.45 nm $S_{0.45}$	0.6 nm $S_{0.6}$	bulk S_{bulk}	0 nm Mb_{dry}	0.45 nm $Mb_{0.45}$	bulk Mb_{bulk}	0 nm MbS_{dry}	0.45 nm $MbS_{0.45}$	bulk MbS_{bulk}
no. of water molecules	0	1083	1706	32400	0	746	9000	0	2788	31793
no. of CTAB molecules	82	82	82	151	0	0	0	289	289	290
no. of Br^- ions	80	82	82	151	0	0	0	284	284	284
no. of SO_4^{2-} ions	0	0	0		2	2	2	2	2	2
total charge	+2	0	0	0	6	−6	−6	−1	−1	0
T_{Final} (K)	280	278	278	*b*	302	249	*b*	306	286	*b*
$\Delta E_{tot}/E_{tot}$ (%)	0.02	0.3	0.2	0.1	0.6	0.1	0.1	0.4	0.2	0.1
N_{Wat}^{evap}	−	110	166	−	−	106	−	−	154	−
N_{Br}^{evap}	0	−	2	−	−	−	−	−	−	−
total simulation time (ns)	20	20	20	50	20	20	10	10	10	65

[a] The simulations are named as follows: Mb, myoglobin; S, surfactant. The subscript denotes vacuum or bulk water or, in the case of a number, the water layer thickness (nanometers). [b] Temperature coupling was used in these simulations, and hence, the final temperature is irrelevant.

micelle can be expected to mimic the polar solvent to some extent, by forming a protective layer around the protein. Separate simulations of isolated surfactant complexes with varying amounts of water are provided as well. Together, these simulations allow us to describe the process of encapsulation of myoglobin in CTAB surfactants during electrospray ionization.

METHODS

To investigate the behavior of surfactant micelles and their effect on protein structure in vacuum, we performed a study in three parts. First, the surfactant and the protein were simulated in two individual systems by themselves and then together as a complex. All simulations were first equilibrated in bulk water, and then starting structures for vacuum simulations were generated. The water molecules were stripped off either entirely or so that just a thin water veil covered the solute. All simulations were performed using the GROMACS package (*18*−*21*). An overview of the simulations, including a naming scheme, is given in Table 1.

CTAB Micelles. An aggregate of 151 CTAB molecules was solvated into a water box with 32400 water molecules (corresponding to a 0.22 M CTAB solution) and simulated for 50 ns (S_{bulk}). The micelle dissociated into two smaller micelles which consisted of 82 and 69 molecules. The larger of these two was extracted after 50 ns for further simulations in vacuum. In those vacuum simulations, the micelle was initially covered with water layers either 0.45 or 0.6 nm in thickness and simulated for 20 ns each. These latter two simulations were named $S_{0.45}$ and $S_{0.6}$, respectively. From the final structure of $S_{0.45}$, the water was removed, and two bromide ions were removed. This system was first simulated with weak position restraints on the nitrogen atoms in the lipid head groups and subsequently for 20 ns without restraints (S_{dry}).

Myoglobin. Horse heart myoglobin [residues 1−152, PDB entry 1DWR (*22*)] with heme and two associated SO_4^{2-} molecules was solvated into 9000 water molecules and was simulated in bulk water for 10 ns (Mb_{bulk}). Virtual hydrogen atoms were used (*23*), allowing a 4 fs integration time step. The "bulk structure" was generated from a cluster analysis (*24*) over the last 8 ns of the trajectory with a cutoff for clustering of 0.1 nm (C_α rmsd). The central structure from the largest cluster (containing 260 of 800 structures) was compared to vacuum structures. Two starting systems for the 20 ns vacuum simulations were generated from the equilibrated final structure. One was surrounded by 746 water molecules ($Mb_{0.45}$, corresponding to a 0.45 nm water layer), and the other had no water at all (Mb_{dry}, 0 nm).

Mb−*CTAB Complex.* The same crystal structure of myoglobin was solvated into a water box with 31793 water molecules and 290 CTAB surfactant molecules. To make the system neutral, six Br^- ions were deleted. This system (MbS_{bulk}) was simulated for 65 ns. The number of water molecules was then reduced to 2788 (equivalent to a 0.45 nm water shell around the protein−surfactant aggregate that had formed), and the simulation was continued using a constant volume (leaving a considerable amount of empty space in the box) for 4 ns, after which a CTAB reverse micelle had formed around the protein. The system was then simulated with ($MbS_{0.45}$) and without (MbS_{dry}) the water under vacuum conditions for 10 ns.

Simulation Specifications. In the simulations, the GROMOS96 43A1 force field (*25*) and, in applicable cases, the SPC water model (*26*) were used. The integration time step was 2 fs in the CTAB simulations and 4 fs in the myoglobin and myoglobin/CTAB simulations.

In the bulk water simulations, periodic boundary conditions were used and the temperature was kept constant at 300 K using Nosé−Hoover coupling (*27, 28*) with a period of 0.5 ps. The pressure was kept constant at 1 bar using Parrinello−Rahman coupling (*29, 30*) with a period of 5 ps. A cutoff of 1 nm was used for the van der Waals interactions. Long-range electrostatic interactions were calculated with the particle mesh Ewald (PME) method (*31, 32*) with a maximum FFT grid spacing of 0.12 nm and cubic interpolation order. Neighbor lists were utilized and updated every fifth integration step, and bond length constraints were applied using the LINCS algorithm (*33*) for the whole system, except water, which was kept rigid using the SETTLE algorithm (*34*). All simulations were parallelized to run on four processors in single-floating point precision.

The systems were energy-minimized before the vacuum simulations and subsequently simulated for 100 ps with the temperature kept constant at 300 K. In the subsequent production simulations, periodic boundary conditions, nonbonded interaction cutoffs, temperature coupling, and pressure coupling were all turned off. Bonds containing hydrogen atoms were constrained using the SHAKE algorithm (*35*) with a relative tolerance of 10^{-8}. The vacuum simulations were run with double precision and in parallel on four processors.

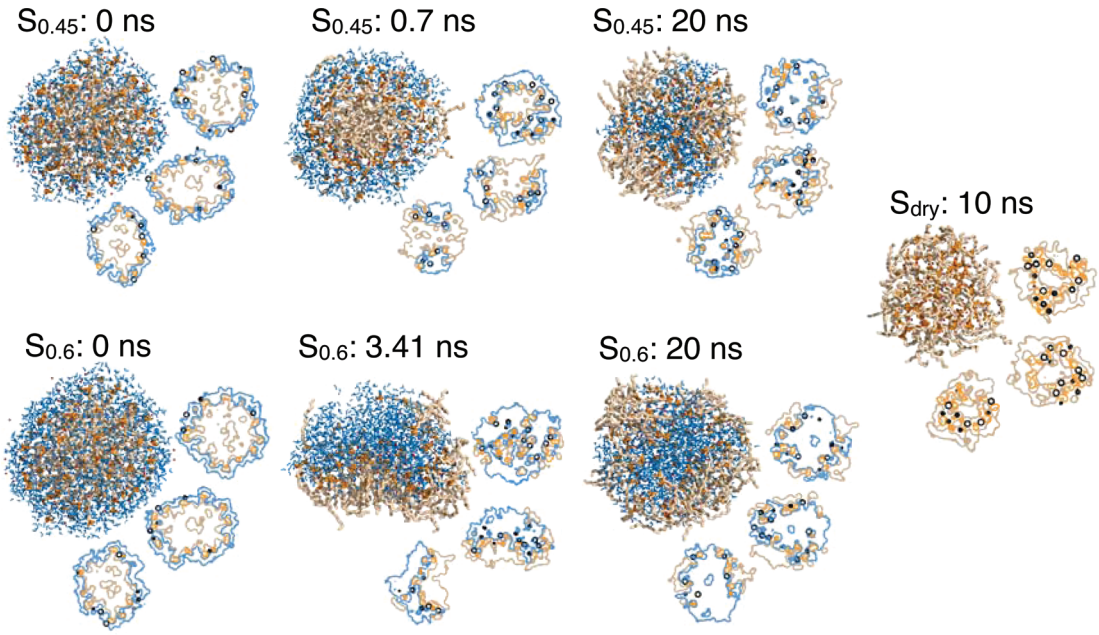

FIGURE 1: CTAB micelles in vacuum, showing the inversion process. To the left are starting structures, intermediate structures, and final structures from $S_{0.45}$ and $S_{0.6}$. To the right is the equilibrium structure from S_{dry}. The smaller tomogram figures show sections through the micelles perpendicular to the principal axes: blue for water, red for Br^-, orange for the head group, and beige for the tail group.

Analysis. The total energy of the simulated systems was monitored to ensure energy conservation ($\Delta E_{tot}/E_{tot}$). To measure temperature changes, it is necessary to have very good energy conservation. Structure analyses of the protein were performed using GROMACS tools and the DSSP program for computing secondary structure of proteins (*36*).

To investigate how the evaporation and phase transition from solution to gas phase affected the protein structure, we computed the following observables from all the simulations: the C_α root-mean-square deviation (rmsd) from the average solution structure, the number of hydrogen bonds within the protein (HB_{pp}) and between the protein and the water (HB_{pw}), the radius of gyration of the protein (R_g), the total (A_{tot}) and hydrophobic (A_{phob}) surface areas of the protein, the protein surface area occluded by surfactant molecules (A_{inter}), the root-mean-square positional fluctuations (rmsf), and the average number of α-helical residues. Hydrogen bonds were defined by a cutoff distance of 0.35 nm and a maximum hydrogen−donor−acceptor angle of 30°. As donor groups, OH and NH groups were used. No distinction was made between the oxygen atoms of the carboxyl groups of aspartates and glutamates and the C-terminus or between the amine groups of arginines. In the analysis of the CTAB micelle, carbons 1−3 and the nitrogen atom were defined as the polar head group, and carbons 5−23 were defined to be the nonpolar tail group.

RESULTS

CTAB Micelles. From an initial aggregate of 151 surfactant molecules in solution, two stable micelles, of 82 and 69 molecules, respectively, formed after 10 ns and remained stable for 40 ns. The larger one, containing 82 CTAB molecules, was selected for the vacuum simulations of the micelle, with two different water layers ($S_{0.45}$ and $S_{0.6}$, respectively, in Table 1) and one without any water (S_{dry}). The S_{dry} simulation was based on the final coordinates from $S_{0.45}$ from which all the water and two of the bromide ions had been removed. The S_{dry} micelle resembles best what was observed in ESI experiments (*17*).

The micelle without any water (S_{dry}) was very stable in vacuum, and the final structure is plotted in Figure 1. Besides normal pictures, we provide "micelle tomograms" (0.1 nm sections through the center of the particle), to allow us to look inside the particle. The S_{dry} micelle forms what looks like a three-layered onion structure with a hydrophobic core and outer layer consisting of the tail groups and a hydrophilic middle layer consisting of the head groups and the counter ions. The water-covered micelles ($S_{0.45}$ and $S_{0.6}$) underwent an inversion where the surfactant reversed orientation from initially having the polar head groups facing outward to having them facing more or less inward. The flip was initialized by the water aggregating, and then a reverse micelle formed around the central water droplet with the polar head groups facing the water and the apolar tails pointing out into the vacuum (Figure 1). As can be seen in the micelle tomograms, in simulation $S_{0.45}$, the water formed a toroid-like arrangement, whereas in simulation $S_{0.6}$, the water formed a more compact body. The inversion process seems to be driven by a drop in the potential energy (Figure 2a), which is superimposed on an overall increase in the potential energy due to evaporation and cooling (Figure 2b).

To follow the inversion process in some more quantitative detail, the moments of inertia for the surfactants were calculated. The moments of inertia significantly increased during this process because the micelle had to expand to be able to accommodate the water (Figure 3). From Figure 1, we can see the process of the micelle transforming from a compact sphere into a reverse micelle with a central cavity filled with water. In this process, the mass distribution of the surfactant molecules moved outward because of the water-filled core, and therefore, the moment of inertia of the surfactant molecules increased temporarily (Figure 3). The duration of the entire inversion process was roughly 1.5 ns ($S_{0.45}$) or 3 ns ($S_{0.6}$). The two systems had different

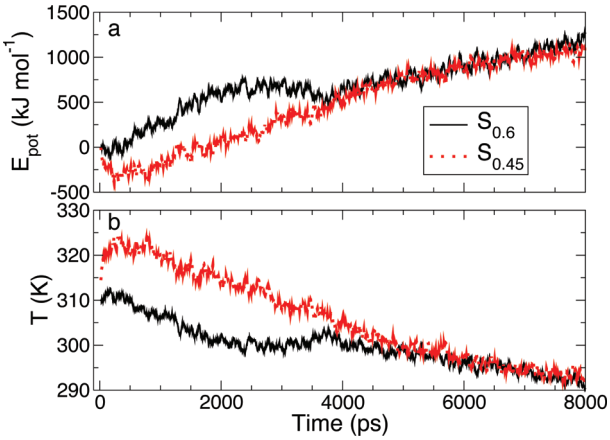

FIGURE 2: (a) Potential energy relative to starting energy and (b) temperature in simulations $S_{0.45}$ and $S_{0.6}$.

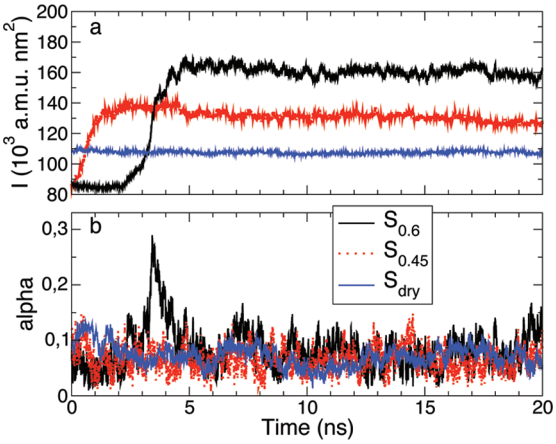

FIGURE 3: (a) Moment of inertia and (b) asymmetry parameter α (eq 1) of the micelle in the CTAB vacuum simulations.

amounts of water, and consequently, one of the micelles expands more than the other and therefore ended up with a larger moment of inertia. We determined the midway time point of the total moment of inertia increase. For the smaller system, this was at ≈0.7 ns and for the larger system at 3.4 ns (Figure 3).

The shape of the surfactant micelle is reflected by the asymmetry parameter (*37*), defined as:

$$\alpha = \frac{2I_1 - I_2 - I_3}{I_1 + I_2 + I_3} \quad (1)$$

where I_1, I_2, and I_3 are the moments of inertia along the principal components vectors, sorted in decreasing order. A small (<0.05) asymmetry parameter value corresponds to a spherical shape. Both the initial right-faced micelle and the final inverted micelle have a high degree of symmetry, but this symmetry temporarily breaks down during the inversion process (Figure 3). Peaks in the asymmetry plots correspond well with the time of inversion as defined by the midpoint of the moment of inertia transition; in the larger system, there is a large peak at 3.4 ns, and in the smaller system, there is a minor peak around 0.5 ns, although the magnitude of this peak is comparable to fluctuation levels during the rest of the simulation (Figure 3).

In total, ∼10% of the water molecules evaporated over the course of 10 ns in simulations $S_{0.45}$ and $S_{0.6}$ (Table 1). Due to the removal of kinetic energy by the evaporating waters, the final temperature decreased to 270 K in both simulations. Two Br^- ions evaporated from the 0.6 nm system, each taking eight water molecules along. It has been found before that ions drag along water molecules when escaping from a water droplet (*38*). In the 0.45 nm system, no ions escaped the cluster during the simulation time.

Myoglobin. Within 2 ns, the Mb in water system (Mb_{bulk}) equilibrated, and the rmsd of the C_α atoms converged to ≈0.13 nm (data not shown). The protein secondary structure is well preserved during the 10 ns simulation. The helical sections changed only slightly during the simulation: there were single-residue shifts in the location of helices A, C, and E; helix E and G were interrupted by a single nonhelical residue; helix F was four residues shorter; and downstream of helix C there was another helix segment, here called C2, from residue 44 to 48, which in the crystal structure was said to consist of two 3_{10} turns (Figure 4).

The protein in water experienced the same types of fluctuations (Figure 5) as the crystal structure used in this work [PDB entry 1DWR (*22*)]. The atomic fluctuations in the crystal showed peaks at the N- and C-termini as well as in loop CD and helix D at residues 44−59, in loop EF and helix F at residues 78−90, and in loop GH near residue 120.

(i) Structural Drift in Vacuo. The structural changes of the protein in vacuum were limited and seemed to be significantly impeded by a thin water film. The dynamics of the protein is illustrated in Figure 6 with the backbone structures from every other nanosecond superimposed on the solvated structure. The dry protein (Mb_{dry}) experienced larger deviations than the water-wrapped one ($Mb_{0.45}$) with some of the α-helices and termini dislocated. For both structures, the turn and helix from residue number 48 to 58 were not as extended as in the equilibrated water structure (Figure 6).

The dry structure experienced fluctuations with peaks in the temperature factor for residues 13, 16, 21, 22, 106, 109, 124, and 129 which were larger than for the solvated structure. The water-covered protein ($Mb_{0.45}$), on the other hand, had very low levels of fluctuation (Figure 5 and Table 2). Also, the rmsd shows that the overall deviation of the water-covered structure was slightly lower than for the dry protein with a mean deviation of the C_α atoms of 0.29 nm ($Mb_{0.45}$) compared to 0.31 nm (Mb_{dry}). The overall size of the proteins, as estimated by the radius of gyration, R_g (Table 2), is somewhat smaller in vacuum, which means that the protein became somewhat more compact during the transition to vacuum. The radius changed from 1.50 nm for the solvated structure (Mb_{bulk}) to 1.48 nm for $Mb_{0.45}$ and 1.46 nm for Mb_{dry}. The solvent accessible surface area (SASA) of the protein was determined using the double-cubed lattice method (*39*). The SASA decreased upon dehydration and showed a pattern similar to that of R_g (Table 2). The effect was milder in the presence of the water film: from 82 nm^2 for Mb_{bulk} to 76 nm^2 for $Mb_{0.45}$ to 67 nm^2 for Mb_{dry}. The hydrophobic surface area is roughly constant in all three simulations in a manner independent of hydration level. It should be noted that the surface area is a property which fluctuates significantly (*40*), and therefore, we explicitly report the standard deviations in Table 2. Figure 6 shows a graphical representation of the surface at the end of the vacuum simulations.

The number of protein intramolecular hydrogen bonds (HB_{pp}) increased in the transition from the solution phase to

FIGURE 4: Eight helices in myoglobin as a function of residue. Average secondary structure as classified by the DSSP algorithm over the last 3 ns for the vacuum simulations and the two bulk simulations. dssp is the classification by the DSSP algorithm on the crystal structure. Evans is the classification by Evans and Grayer (*42*).

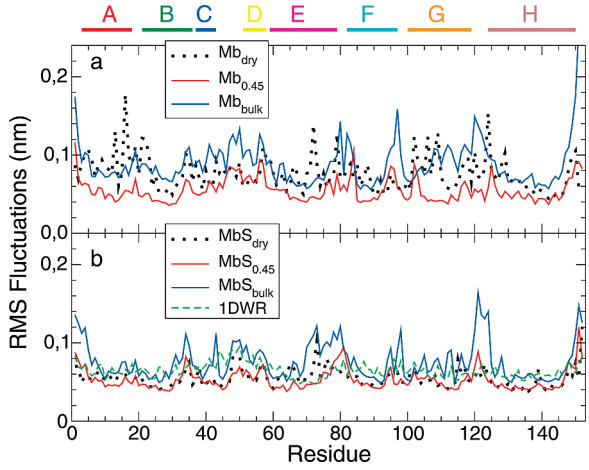

FIGURE 5: Temperature factors calculated for the protein atoms on a per residue basis for the last 3 ns of the vacuum simulations for the system (a) without surfactants and (b) with surfactants. 1DWR indicates fluctuations computed from the average *B* factor per residue from the starting structure used for our simulations. The positions of the helices in the crystal structure are given at the top.

the vacuum phase (Table 2). HB_{pp} increases sharply to 161 for the Mb_{dry} simulation and more moderately to 127 in $Mb_{0.45}$ (compared to 123 in Mb_{bulk}). In the solvated vacuum structure ($Mb_{0.45}$), the loss of 34 hydrogen bonds between the protein and water [HB_{pw} (Table 2)] is offset to some extent by the formation of four new intramolecular hydrogen bonds (replacing eight hydrogen bonds with water). The dry structure on the other hand could not form enough intramolecular hydrogen bonds to make up for all of the lost interactions with the water.

There is a clear change in the helix structure when all water is removed. Helix A was reduced in length from 16 residues in the bulk water and crystal structures to just three in vacuum with no water. Helices E and G were also both reduced to less than half the size. Helix F on the other hand experienced a stabilizing effect and was extended, although the size of this helix seemed to be highly dependent on the environment, and indeed, it is less stable in solution than in the crystal (Figure 4). The total number of α-helical residues was reduced to only half compared to the number in the water-equilibrated structure (Table 2), and many of the remaining residues were of the 3_{10} type.

The 0.45 nm water layer protects the helices of the protein remarkably well and the structure showed only minor fluctuations (Figure 5a). The most significant difference from the bulk water simulation was the extension of the C-terminal H helix. From $Mb_{0.45}$ 106 of the water molecules evaporated during the 20 ns of simulation, corresponding to 14% of the total number (Table 1). The temperatures decreased due to the evaporation and converged to 249 K after 10 ns.

Mb−CTAB Complex in Solution and in Vacuo. (i) Aggregation of the Protein and Surfactants. The CTAB surfactants did not form a complete reverse micelle around the myoglobin in bulk water within 65 ns of simulation; however, the contact area increases significantly during the simulation (Figure 7). The aggregates that formed between the protein and the surfactant molecules consist of smaller micellar structures in association to the protein (Figure 6). To create true micelles, the amount of water was reduced so that only a 0.45 nm water shell around the aggregate was left, leaving some vacuum in the simulation box. This system was simulated (with periodic boundary conditions and constant volume) for 4 ns, and in that time, a reverse micelle formed spontaneously around the protein (Figure 6). This structure was then used for subsequent simulations in vacuo.

(ii) Preservation of the Protein Structure in Vacuo. The structure of myoglobin was quite stable when encapsulated in a surfactant layer shielding the protein from vacuum. The backbone of the protein is very similar to the one from the equilibrated water structure in both simulations as shown in columns c and d of Figure 6, and the fluctuations are small as well (Figure 5). The C_α rmsd values on the other hand are significant, and ∼0.3 nm, independent of the amount of water (Table 2).

The secondary structure stayed very close to the bulk water structure for both systems. In the system with no water (MbS_{dry}), helices G and H were shortened slightly and the region of residues 44−48 which is difficult to classify structurally had some helicity in $MbS_{0.45}$ but not in MbS_{dry}. Other than that, there were only differences of single residues compared to the solvated structure. The DSSP algorithm (*36*) classified 110 of the residues as being α-helical in the water-equilibrated structure. It is well-known that assignment of secondary structure in helix termini is somewhat arbitrary (*41*), and hence, we conclude that the differences between the secondary structure assigned by DSSP (117) and a human [134 (*42*)] are not very significant (Figure 4). This notion validates comparison between the bulk secondary structure and that in other simulations, as long as the assignment is done in the same manner in all cases. In simulation $MbS_{0.45}$, 108 residues were classified as α-helical versus 97 in simulation MbS_{dry}. The number of intramolecular hydrogen bonds in myoglobin within the CTAB micelle is virtually identical to that in the solvated protein structure, ∼123 in all cases (Table 2).

In complex with the surfactants, the protein "inflates" somewhat, as seen in a slightly larger radius of gyration and a considerably increased solvent accessible surface area (Table 2). The total surface area increased to ∼99 nm^2 in MbS_{bulk} compared to 82 nm^2 in the solvated structure Mb_{bulk}

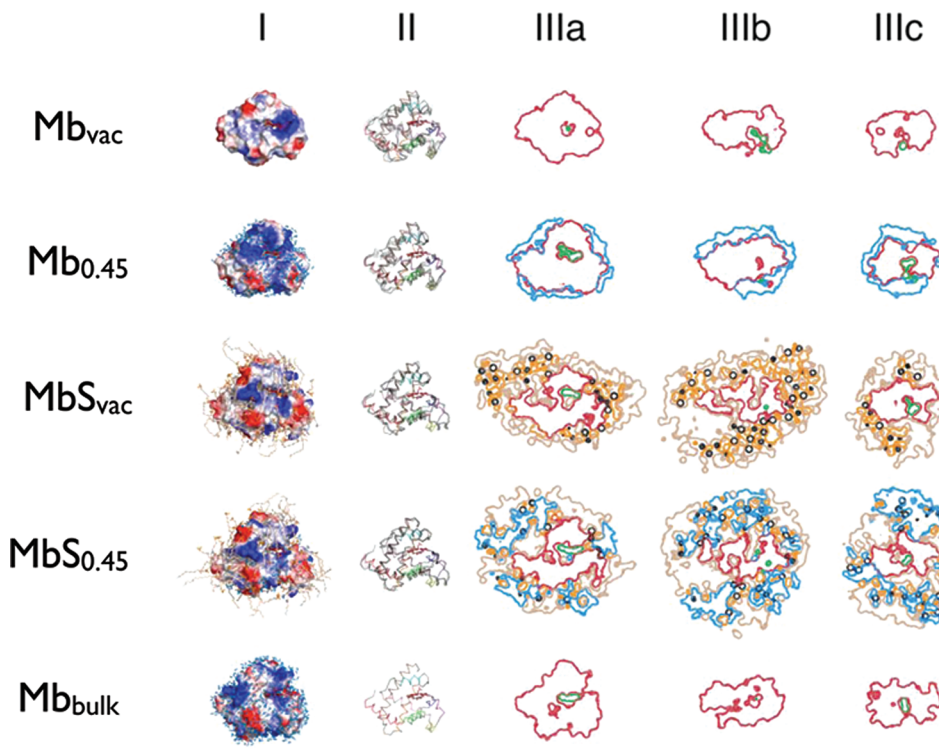

FIGURE 6: Protein structure in vacuum with a reference bulk water-equilibrated structure. (I) Charge distribution at the solvent accessible surfaces and distribution of water (blue) and/or CTA molecules (orange and beige) within 0.4 nm for the final vacuum structures. Red indicates negative, blue positive, and white neutral. The heme group is colored red. (II) Ten snapshots of the backbone structure (black) taken equidistantly spaced throughout the vacuum trajectories superimposed on the water-equilibrated structure colored according to the color scheme of Figure 4. The heme group is colored red. (III) Thin slices (0.1 nm) through the systems orthogonal to principal component vectors 1 and 2 (a), 1 and 3 (b), and 2 and 3 (c). Protein is colored red and water blue, and surfactant head groups are colored orange, surfactant tail groups brown, and Br^- ions black. Heme is colored green.

Table 2: Structural Properties of the Protein in the Simulation[a]

	Mb_{dry}	$Mb_{0.45}$	Mb_{bulk}	MbS_{dry}	$MbS_{0.45}$	MbS_{bulk}
rmsd (nm)	0.31(1)	0.29(1)	0.11(1)	0.31(1)	0.31(1)	0.30(1)
HB_{pp}	161(6)	127(4)	123(5)	122(4)	124(4)	122(4)
HB_{pw}	–	245(8)	279(10)	–	73(5)	96(6)
R_g (nm)	1.46(1)	1.48(1)	1.50(1)	1.58(1)	1.59(1)	1.59(1)
A_{tot} (nm^2)	67(1)	76(1)	82(2)	97(1)	96(1)	99(2)
A_{phob} (nm^2)	47(1)	44(1)	46(1)	60(1)	59(1)	61(2)
A_{inter} (nm^2)	–	–	–	80(1)	73(1)	68(2)
rmsf (nm)	0.055(1)	0.053(1)	0.076(2)	0.076(2)	0.055(1)	0.091(3)
N_α	52(5)	104(3)	111(3)	97(3)	108(3)	106(3)

[a] Root-mean-square deviation of the C_α atoms compared to the average water-equilibrated structure, the number of hydrogen bonds within the protein and between the protein and water, the radius of gyration, the total and hydrophobic surface area of the protein, the interaction area between the protein and surfactants, the average root-mean-square position fluctuation, and the number of residues classified as belonging to an α-helix. Values are time averages over the last 3 ns of the simulations. Numbers in parentheses are the standard deviations in the last digit.

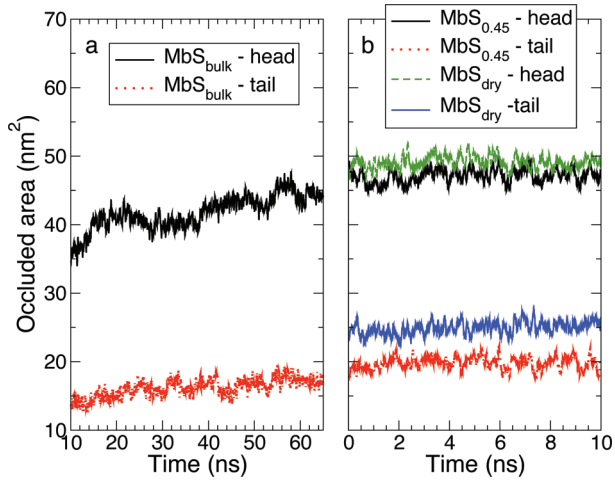

FIGURE 7: Area of interaction between surfactants and protein. (a) Surfactant head groups and (b) surfactant tails. Black lines show 200-point running averages.

without surfactants. The surface areas are virtually identical in all simulations with surfactants (Table 2).

The reverse micelle remained stable throughout the whole vacuum simulation with the polar head groups predominantly facing inward and the apolar tails facing the vacuum. This was the case both with ($MbS_{0.45}$) and without (MbS_{dry}) water (Figure 6). The micelle adopted a more compact shape in vacuum, with an initial decrease in the moment of inertia *I*, roughly 10% within the first couple of nanoseconds, after which it leveled off (Figure 8). System $MbS_{0.45}$ had a higher degree of symmetry, as measured by the asymmetry parameter α (eq 1), than MbS_{dry}. At the end of 10 ns, it had adopted an almost perfect spherical shape. The dry system (MbS_{dry}) had a slightly elongated shape.

For each residue in the protein, the number of surfactant atoms within 0.6 nm was computed, based on radial distribution functions and separately for head group atoms and tail atoms (Figure 9). The number of contacts increases significantly upon going from bulk (MbS_{bulk}) to a water layer ($MbS_{0.45}$) to a dry system (MbS_{dry}). For the head group atoms, patterns showing two residues with a large number of contacts followed by two residues with few contacts are revealed. This pattern distinguishes the outward-facing residues from the buried residues in an α-helix. The surface

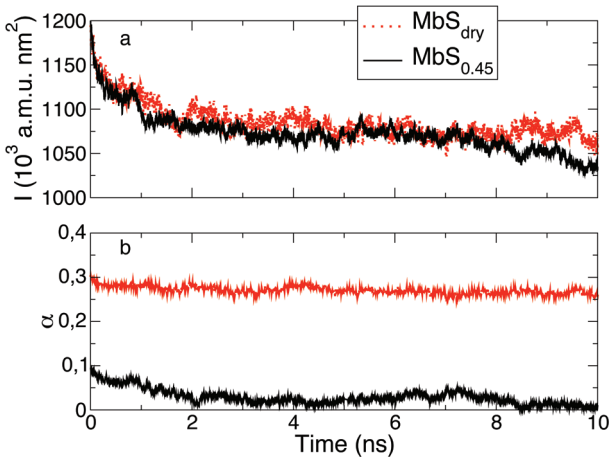

FIGURE 8: (a) Moments of inertia and (b) asymmetry parameter α (eq 1) values of the micelle for the myoglobin−CTAB vacuum simulations.

area of the protein that is occluded by the surfactants was computed using the double-cube lattice method (*39*) (Figure 7), again separately for head groups and tail atoms. In both the MbS_{dry} and $MbS_{0.45}$ simulations, these areas are at a constant high level of roughly 96 nm^2. In MbS_{bulk}, we see a slow increase of the area over 65 ns, and the occluded area between head groups and protein in MbS_{bulk} approaches that in $MbS_{0.45}$, confirming that the solution structure (with lipids) is similar to a gas phase complex (*17*), at least when some water is present. A further tomogram analysis was made showing cross sections through the protein in complex with water and/or surfactants. The protein was oriented along its principal axes before the cross sections were made (Figure 6). In this manner, we can dissect, at least qualitatively, the interactions and structure of the complexes. Indeed, the different molecules are intertwined in a complex manner; for instance, in view IIIc of MbS_{dry}, we can see surfactant tails close to the core of the protein.

A total of 154 water molecules, corresponding to 5.5%, evaporated during simulation $MbS_{0.45}$, and the temperature fell to 286 K. The total energy was well-conserved with a $\Delta E_{tot}/E_{tot}$ of 0.2%. System MbS_{dry} experienced a slight (2%) increase in temperature, due to formation of the more favorable conformation of the complex, which is associated with a lower potential energy. No Br^- ions evaporated in either of the systems.

DISCUSSION

Hydration of myoglobin has been studied extensively by a combination of X-ray crystallography, neutron scattering, and molecular simulation (*43*−*51*). Most of these studies were aimed at explaining the specific hydration sites present in crystal structures of Mb, i.e., in solution. Early work by Steinbach and others revealed that in case myoglobin is solvated by a limited number of water molecules, these waters tend to bind to charged and polar groups (*43, 45*). Lounnas et al. estimated that roughly 500 water molecules are tightly bound to Mb (*46*), a number that is very well comparable to what we used in our simulation of Mb with a 0.45 nm water shell (746), of which 106 molecules evaporated after 10 ns, leaving 640 bound molecules (Table 1). Obviously, the number of bound water molecules and their preferred locations are related to the size and local polarity of the surface.

CTAB Micelles Invert When They Are Dehydrated. The critical micelle concentration (CMC) for CTAB has experimentally been determined to lie in the interval of 0.89−0.93 mM (*52*); this property obviously depends on factors such as the temperature and the presence of other molecules. The effective starting concentration of CTAB in our simulation

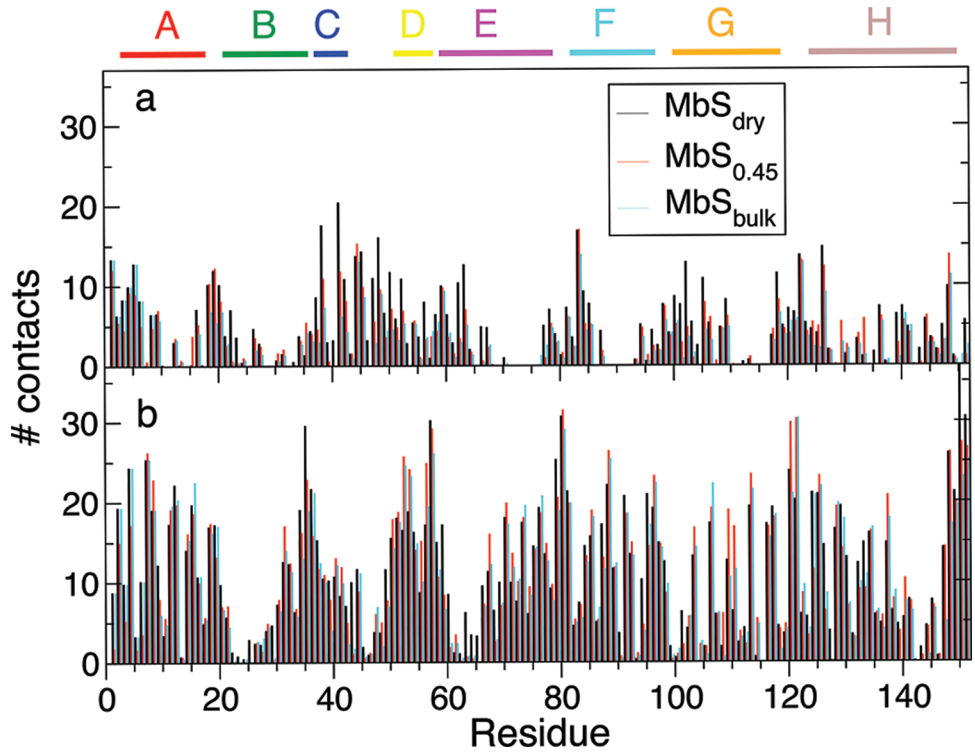

FIGURE 9: Number of contacts within 0.6 nm, between Mb and (a) surfactant head groups and (b) surfactant tails, summed per residue. The positions of the helices in the crystal structure are given at the top.

(S_{bulk}) was 0.22 M to promote the spontaneous formation of micelles, which is fine since we are not dealing with the kinetics of micelle formation in this work (*53*). Hence, CTAB molecules readily formed micelle complexes within 10 ns. These initial micelles were large and unstable. A micelle of 151 molecules broke up into two smaller micelles of 82 and 69 molecules, which stayed intact for 40 ns, until the end of simulation S_{bulk}. The size of these micelles agrees with experimental figures which state that the aggregation number of CTAB micelles lies in the interval of 60−89 surfactant molecule per micelle (*52*). This shows that our simulations correctly reproduce the aggregation behavior of CTAB molecules in water.

The larger of the two stable micelles was used to study the behavior of a CTAB micelle during ESI conditions. The dehydration process was mimicked with water layers of different thicknesses. The micelles seem to have an intrinsic propensity to invert into a reverse micelle when put into a vacuum environment (Figure 1). During the inversion step, there is a sharp increase in the number of water−water hydrogen bonds and interactions between the polar head groups and water, which obviously is the driving force for the inversion (Figure 2). The polar head groups of the surfactant molecules interact with the water and form a layer around the water core of the droplet, while the hydrophobic tail groups are predominantly arranged on the surface of the particle. The S_{dry} micelle has a three-layered structure (Figure 1). Although the possibility that regular micelles can be produced under very gentle conditions in an ESI cannot be rigorously excluded, there is no direct evidence to prove their existence. Sharon et al. argue that bromide ions are exchanged for acetate ions, which can readily happen in solution; however, this does not prove that CTA−acetate complexes do not invert when transferred into the gas phase, as is shown for simulations of CTAB molecules here (Figure 1).

Myoglobin Associates with Surfactants in Solution. As would be expected, there did not seem to be any tendency for the surfactants to spontaneously form a complete reverse micelle around the water soluble protein. Still, considerable aggregation of the surfactant and the protein took place (Figure 7). In particular, the occluded surface area between protein and head groups is almost as large in MbS_{bulk} as in $MbS_{0.45}$, whereas the contact area between surfactant tails and protein is somewhat smaller. The area is still considerably smaller than in MbS_{dry} though. An alternative to promoting the formation of a reverse micelle would be to use an apolar solvent. Sharon et al. (*17*) constructed protein−surfactant complexes with one protein associated with 230−317 CTAB molecules using a hexanol/water mixture. There is of course a risk of partially denaturing the protein during such a process. We mimicked the evaporation process that would take place during ESI by reducing the amount of water, and here, the protein−surfactant aggregate readily formed a reverse micelle with the protein incorporated in the middle.

The Structure Drift of the Protein Is Suppressed by Encapsulation. The backbone structures from the four vacuum simulations are similar to varying degrees to the solvated structure (Figure 6). The largest deviations are found for the completely naked protein [Mb_{dry} (Figure 6)]. The structures for the water-covered protein ($Mb_{0.45}$) and the protein engulfed by a CTAB micelle (MbS_{dry}) were more "nativelike". The "best" vacuum structure in this respect was that of the protein in complex with surfactant molecules with residual water present ($MbS_{0.45}$) which displayed an average C_α rmsd of 0.3 nm with respect to the solvated structure (Table 2) but had all helices intact (Figure 4).

From the DSSP (*36*) classification (Table 2 and Figure 4), it appears that solvation by water contributes significantly to the preservation of secondary structure. The number of α-helix residues in $Mb_{0.45}$ and $MbS_{0.45}$ was almost as high as in the solvated structure and the crystal structure. Horse heart myoglobin has eight helices (A−H) in the crystal structure which together constitute 131 of 153 residues, all of them α-helices, except helix C which is a 3_{10}-helix. The DSSP algorithm judges the crystal structure somewhat differently than the original authors, by classifying only 114 of the residues as α-helical. Such differences are well-documented (*41*) and lie predominantly at the ends of the helices (Figure 4). All eight α-helices were intact throughout the vacuum simulations, but in some cases, they degraded in the ends or were disrupted by a non-α-helical residue (Figure 4). The largest deviations were found in the loop regions which also have high temperature factors in the crystal structure. Apart from the fact that there were two segments which had different morphologies under different conditions. The long curved section that connects helix B and helix E consists in the crystal of a short 3_{10}-helix (residues 36−43), followed by two 3_{10}-turns (residues 43−46 and 46−49) and finally a short α-helix (residues 51−58). The two 3_{10}-turns adopt an α-helical structure when the protein is equilibrated in bulk water. This helix was also found in both of the vacuum structures which contained water ($Mb_{0.45}$ and $MbS_{0.45}$) as well as the structure with just CTAB surfactant (MbS_{dry}). The turn between helices E and F was minimal in the crystal with just one residue between the helices. In the bulk water simulation, the turn grew at the expense of the helices. The same happened in all three vacuum structures which had either water or surfactant.

The myoglobin structure expands somewhat in vacuum when incorporated in a CTAB micelle. The solvent accessible surface area increases by up to 25% for those two systems. Because the area to volume ratio is very high with numerous small protruding extensions and grooves, a slight change in the position of surface elements has a large effect on the surface area. The proximity of the aliphatic chains of the surfactant may induce the hydrophobic core of the protein. The fraction hydrophobic surface area did not change significantly, so the expansion of Mb is not biased toward an increased hydrophobic surface area. The protein without the CTAB micelle showed the opposite behavior with a decrease in the surface area when exposed to vacuum. This effect was most obvious when no water film was present. Weak interactions such as van der Waals interactions will play a somewhat larger role when there are no solvent molecules present that can solvate protruding arms of the protein. The dominant effect, however, is electrostatic in nature which can be seen from the increase in the number of intramolecular hydrogen bonds (Table 2).

In all of the simulation systems in vacuum which contained water, there was a limited degree of evaporation of water molecules, and in $MbS_{0.45}$, two Br^- ions evaporated as well, each taking eight water molecules along. The evaporation

followed the same pattern that has been described previously for similar systems (*9, 38, 54*).

CONCLUSION

The combination of mass spectrometry and molecular simulation has proven to be a very powerful way of studying biomolecules in the gas phase (*6*−*10, 55*−*57*). Here we have shown that CTAB reverse micelles, generated in vacuo in a "gentle" source, like ESI (*4*), form almost perfect spherical aggregates, either with or without solvent (Figure 1). Myoglobin is encapsulated effectively in surfactant (reverse) micelles, and inside this "packaging", the protein structure is very similar to the bulk structure (Figures 4 and 6). In a previous study of proteins covered by water shells in the gas phase (*9*) as well as in this work, we have shown that a thin layer of residual water provides protection from the nonphysiological vacuum environment. Although it is known that, for example, virus particles can traverse air or even vacuum (*58*) and still be infective, it is obvious that the conformation of surface residues must be affected to some degree, and it can be expected that this is more severe for small particles than for large ones. On the other hand, even a protein as small as the Trp cage shows remarkable stability, even at high temperatures, in unfolding studies in the gas phase (*59, 60*), so a general answer about the degree of conformational changes in biomolecules due to the vacuum environment cannot be given at this point in time. From our results, we conclude that preserving a layer of water or other molecules like surfactants on the protein in mass spectrometry experiments would significantly increase the biological relevance of the results. Finally, in the context of X-ray free electron laser bioimaging, it is promising to note that different routes to encapsulating proteins give comparable protection against structural changes. Suggestions have been made that such a "tamper" layer might protect the particle from radiation damage as well (*2, 14*).

ACKNOWLEDGMENT

We acknowledge stimulating discussions with Carl Caleman and Erik Marklund.

REFERENCES

1. Barrera, N. P., Bartolo, N., Booth, P. J., and Robinson, C. V. (2008) Micelles protect membrane comlexes from solution to vacuum. *Science 321*, 243–246.
2. Neutze, R., Wouts, R., van der Spoel, D., Weckert, E., and Hajdu, J. (2000) Potential for biomolecular imaging with femtosecond X-ray pulses. *Nature 406*, 752–757.
3. Neutze, R., Huldt, G., Hajdu, J., and van der Spoel, D. (2004) Potential impact of an X-ray free electron laser on structural biology. *Radiat. Phys. Chem. 71*, 905–916.
4. Fenn, J. B., Mann, M., Meng, C. K., Wong, S. F., and Whitehouse, C. M. (1989) Electrospray ionization for mass spectrometry of large biomolecules. *Science 246*, 64–71.
5. Bruins, A. P. (1998) Mechanistic aspects of electrospray ionization. *J. Chromatogr., A 794*, 345–357.
6. Mao, Y., Ratner, M. A., and Jarrold, M. F. (1999) Molecular dynamics simulations of the charge-induced unfolding and refolding of unsolvated cytochrome [c]. *J. Phys. Chem. B 103*, 10017–10021.
7. Jarrold, M. F. (1999) Unfolding, refolding and hydration of protein ions in the gas phase. *Acc. Chem. Res. 32*, 360–367.
8. Mao, Y., Ratner, M. A., and Jarrold, M. F. (2001) Molecular dynamics simulations of the rehydration of folded and unfolded cytochrome C ions in the vapor phase. *J. Am. Chem. Soc. 123*, 6503–6507.
9. Patriksson, A., Marklund, E., and van der Spoel, D. (2007) Protein conformations under electrospray conditions. *Biochemistry 46*, 933–945.
10. Patriksson, A., Adams, C., Kjeldsen, F., Zubarev, R. A., and van der Spoel, D. (2007) A direct comparison of protein structure in gas and solution phase: The Trp-cage. *J. Phys. Chem. B 111*, 13147–13150.
11. Konermann, L. (2007) A minimalist model for exploring conformational effects on the electrospray charge state distribution of proteins. *J. Phys. Chem. B 111*, 6534–6543.
12. Robinson, C. V., Chung, E. W., Kragelund, B. B., Knudsen, J., Aplin, R. T., Poulsen, F. M., and Dobson, C. M. (1996) Probing the nature of non-covalent protein ligand interactions by mass spectrometry. *J. Am. Chem. Soc. 118*, 8646–8653.
13. Hau-Riege, S. P., Szoke, H., Chapman, H. N., Szoke, A., Marchesini, S., Noy, A., He, H. F., Howells, M., Weierstall, U., and Spence, J. C. H. (2004) Speden: Reconstructing single particles from their diffraction patterns. *Acta Crystallogr. A4*, 294–305.
14. Hau-Riege, S. P., London, R. A., Chapman, H. N., Szoke, A., and Timneanu, N. (2007) Encapsulation and diffraction-pattern-correction methods to reduce the effect of damage in X-ray diffraction imaging of single biological molecules. *Phys. Rev. Lett. 98*, 198302.
15. Abramson, J., Larsson, G., Byrne, B., Puustinen, A., Garcia-Horsman, A., and Iwata, S. (2000) Purification, crystallization and preliminary crystallographic studies of an integral membrane protein, cytochrome bo_3 ubiquinol oxidase from *Escherichia coli*. *Acta Crystallogr. D8*, 1076–1078.
16. Kashino, Y. (2003) Separation methods in the analysis of protein membrane complexes. *J. Chromatogr., B 797*, 191–216.
17. Sharon, M., Ilag, L. L., and Robinson, C. V. (2007) Evidence of micellar structure in the gas phase. *J. Am. Chem. Soc. 129*, 8740–8746.
18. Berendsen, H. J. C., van der Spoel, D., and van Drunen, R. (1995) GROMACS: A message-passing parallel molecular dynamics implementation. *Comput. Phys. Commun. 91*, 43–56.
19. Lindahl, E., Hess, B. A., and van der Spoel, D. (2001) GROMACS 3.0: A package for molecular simulation and trajectory analysis. *J. Mol. Model. 7*, 306–317.
20. van der Spoel, D., Lindahl, E., Hess, B., Groenhof, G., Mark, A. E., and Berendsen, H. J. C. (2005) GROMACS: Fast, Flexible and Free. *J. Comput. Chem. 26*, 1701–1718.
21. Hess, B., Kutzner, C., van der Spoel, D., and Lindahl, E. (2008) Gromacs 4.0: Algorithms for highly efficient, load-balanced, and scalable molecular simulation. *J. Chem. Theor. Comput. 4*, 435–447.
22. Chu, K., Vojtchovsky, J., McMahon, B. H., Sweet, R. M., Berendzen, J., and Schlichting, I. (2000) Structure of a ligand-binding intermediate in wild-type carbonmonoxy myoglobin. *Nature 403*, 921–923.
23. Feenstra, K. A., Hess, B., and Berendsen, H. J. C. (1999) Improving efficiency of large time-scale molecular dynamics simulations of hydrogen-rich systems. *J. Comput. Chem. 20*, 786–798.
24. Daura, X., Gademann, K., Jaun, B., Seebach, D., van Gunsteren, W. F., and Mark, A. E. (1999) Peptide folding: When simulation meets experiment. *Angew. Chem., Int. Ed. 38*, 236–240.
25. van Gunsteren, W. F., Billeter, S. R., Eising, A. A., Hünenberger, P. H., Krüger, P., Mark, A. E., Scott, W. R. P., and Tironi, I. G. (1996) *Biomolecular Simulation: The GROMOS96 manual and user guide*, Hochschuleverlag AG an der ETH Zürich, Zürich.
26. Berendsen, H. J. C., Postma, J. P. M., van Gunsteren, W. F., and Hermans, J. (1981) in *Intermolecular Forces* (Pullman, B., Eds.) pp 331−342, D. Reidel Publishing Co., Dordrecht, The Netherlands.
27. Nosé, S. (1984) A molecular dynamics method for simulations in the canonical ensemble. *Mol. Phys. 52*, 255–268.
28. Hoover, W. G. (1985) Canonical dynamics: Equilibrium phase-space distributions. *Phys. Rev. A 31*, 1695–1697.
29. Parrinello, M., and Rahman, A. (1981) Polymorphic transitions in single crystals: A new molecular dynamics method. *J. Appl. Phys. 52*, 7182–7190.
30. Nosé, S., and Klein, M. L. (1983) Constant pressure molecular dynamics for molecular systems. *Mol. Phys. 50*, 1055–1076.
31. Darden, T., York, D., and Pedersen, L. (1993) Particle mesh Ewald: An N-log(N) method for Ewald sums in large systems. *J. Chem. Phys. 98*, 10089–10092.
32. Essmann, U., Perera, L., Berkowitz, M. L., Darden, T., Lee, H., and Pedersen, L. G. (1995) A smooth particle mesh Ewald method. *J. Chem. Phys. 103*, 8577–8592.

33. Hess, B., Bekker, H., Berendsen, H. J. C., and Fraaije, J. G. E. M. (1997) LINCS: A linear constraint solver for molecular simulations. *J. Comput. Chem. 18*, 1463–1472.
34. Miyamoto, S., and Kollman, P. A. (1992) SETTLE: An analytical version of the SHAKE and RATTLE algorithms for rigid water models. *J. Comput. Chem. 13*, 952–962.
35. Ryckaert, J. P., Ciccotti, G., and Berendsen, H. J. C. (1977) Numerical integration of the cartesian equations of motion of a system with constraints: Molecular dynamics of n-alkanes. *J. Comput. Phys. 23*, 327–341.
36. Kabsch, W., and Sander, C. (1983) Dictionary of protein secondary structure: Pattern recognition of hydrogen-bonded and geometrical features. *Biopolymers 22*, 2577–2637.
37. Tieleman, D. P., van der Spoel, D., and Berendsen, H. J. C. (2000) Molecular dynamics simulations of dodecylphosphocholine micelles at three different aggregate sizes: Micellar structure and chain relaxation. *J. Phys. Chem. B 104*, 6380–6388.
38. Caleman, C., and van der Spoel, D. (2007) Evaporation from water clusters containing singly charged ions. *Phys. Chem. Chem. Phys. 37*, 5105–5111.
39. Eisenhaber, F., Lijnzaad, P., Argos, P., Sander, C., and Scharf, M. (1995) The double cube lattice method: Efficient approaches to numerical integration of surface area and volume and to dot surface contouring of molecular assemblies. *J. Comput. Chem. 16*, 273–284.
40. Novotny, M., Seibert, M., and Kleywegt, G. J. (2007) On the precision of calculated solvent-accessible surface areas. *Acta Crystallogr D63*, 270–274.
41. Martin, J., Letellier, G., Marin, A., Taly, J. F., de Brevern, A. G., and Gibrat, J. F. (2005) Protein secondary structure assignment revisited: A detailed analysis of different assignment methods. *BMC Struct. Biol. 5*, 17.
42. Evans, S. V., and Brayer, G. D. (1990) High-resolution study of the three-dimensional structure of horse heart metmyoglobin. *J. Mol. Biol. 213*, 885–897.
43. Steinbach, P. J., Loncharich, R. J., and Brooks, B. R. (1991) The effects of environment and hydration on protein dynamics: A simulation study of myoglobin. *Chem. Phys. 158*, 383–394.
44. Lounnas, V., Pettitt, B. M., Findsen, L., and Subramaniam, S. (1992) A microscopic view of protein solvation. *J. Phys. Chem. 96*, 7157–7159.
45. Steinbach, P. J., and Brooks, B. R. (1993) Protein hydration elucidated by molecular-dynamics simulation. *Proc. Natl. Acad. Sci. U.S.A. 90*, 9135–9139.
46. Lounnas, V., and Pettitt, B. M. (1994) A connected cluster of hydration around myoglobin: Correlation between molecular-dynamics simulations and experiment. *Proteins 18*, 133–147.
47. Gu, W., and Schoenborn, B. P. (1995) Molecular-dynamics simulation of hydration in myoglobin. *Proteins 22*, 20–26.
48. Lindahl, E., and Edholm, O. (1998) Solvent diffusion outside macromolecular surfaces. *Phys. Rev. E 57*, 791–796.
49. Makarov, V. A., Andrews, B. K., Smith, P. E., and Pettitt, B. M. (2000) Residence times of water molecules in the hydration sites of myoglobin. *Biophys. J. 79*, 2966–2974.
50. Henchman, R. H., and McCammon, J. A. (2002) Extracting hydration sites around proteins from explicit water simulations. *J. Comput. Chem. 23*, 861–869.
51. Doster, W., and Settles, M. (2005) Protein-water displacement distributions. *Biochim. Biophys. Acta 1749*, 173–186.
52. Feitosa, E., Brazolin, M. R. S., Naal, R. M. Z. G., Lama, M. P. F. M. D., Lopes, J. R., Loh, W., and Vasilescu, M. (2006) Structural organization of cetyltrimethylammonium sulfate in aqueous solution: The effect of Na_2SO_4. *J. Colloid Interface Sci. 299*, 883–889.
53. Marrink, S. J., Tieleman, D. P., and Mark, A. E. (2000) Molecular dynamics simulation of the kinetics of spontaneous micelle formation. *J. Phys. Chem. B 104*, 12165–12173.
54. Caleman, C., and van der Spoel, D. (2006) Temperature and structural changes of water clusters in vacuum due to evaporation. *J. Chem. Phys. 125*, 154508.
55. Jarrold, M. F. (2000) Peptides and proteins in the vapor phase. *Annu. Rev. Phys. Chem. 51*, 179–207.
56. Patriksson, A., Adams, C., Kjeldsen, F., Raber, J., van der Spoel, D., and Zubarev, R. A. (2006) Prediction of N-C_α bond cleavage frequencies in electron capture dissociation of Trp-cage dications by force-field molecular dynamics simulations. *Int. J. Mass Spectrom. 248*, 124–135.
57. Adams, C. M., Kjeldsen, F., Patriksson, A., van der Spoel, D., Gräslund, A., Papadopoulos, E., and Zubarev, R. A. (2006) Probing solution- and gas-phase structures of trp-cage cations by chiral substitution and spectroscopic techniques. *Int. J. Mass Spectrom. 253*, 263–273.
58. Tito, M. A., Tars, K., Valegård, K., Hajdu, J., and Robinson, C. V. (2000) Electrospray time of flight mass spectrometry of the intact MS2 virus capsid. *J. Am. Chem. Soc. 122*, 3550–3551.
59. Iavarone, A., and Parks, J. (2005) Conformational change in unsolvated trp-cage protein probed by fluorescence. *J. Am. Chem. Soc. 127*, 8606–8607.
60. Iavarone, A., Patriksson, A., van der Spoel, D., and Parks, J. (2007) Fluorescence probe of trp-cage protein conformation in solution and in gas-phase. *J. Am. Chem. Soc. 129*, 6726–6735.

BI801952F